

# Anisotropic Superparamagnetism of Monodisperse Cobalt-Platinum Nanocrystals

F. Wiekhorst,<sup>1</sup> E. Shevchenko,<sup>2</sup> H. Weller,<sup>2</sup> and J. Kötzler<sup>1</sup>

<sup>1</sup>*Institut für Angewandte Physik und Zentrum für Mikrostrukturforschung,  
Universität Hamburg, Jungiusstrasse 11, D-20355 Hamburg, Germany*

<sup>2</sup>*Institut für Physikalische Chemie, Universität Hamburg, Bundesstrasse 45, D-20146 Hamburg  
(Dated: January 29, 2020)*

Based on the high-temperature organometallic route (Sun *et al.* Science **287**, 1989 (2000)), we have synthesized powders containing capped CoPt<sub>3</sub> single crystals with mean diameters of 3.3(2) nm and 6.0(2) nm and small log-normal widths  $\sigma=0.15(1)$ . In the entire temperature range from 5 K to 400 K, the DC-susceptibility  $\chi(T)$  displays significant deviations from ideal superparamagnetism. Approaching the Curie temperature of 450(10) K, this is due to the (mean-field) type reduction of the ferromagnetic moments, while below the blocking temperature  $T_b$ ,  $\chi(T)$  is suppressed by the presence energy barriers, the distributions of which scale with the particle sizes. Scaling analyses of the shape of the magnetic absorption  $\chi''(T, \omega)$  reveals distribution functions for the barriers consistent with those from transmission electron microscopy. Above 200 K, the magnetization isotherms  $M(H, T)$  display Langevin behavior providing 2.5(1)  $\mu_B$  per CoPt<sub>3</sub> in agreement with reports on bulk and thin film CoPt<sub>3</sub>. The non-Langevin shape at lower temperatures is for the first time interpreted by taking into account an anisotropy energy of the nanoparticles  $E_A(T)$ . Using the magnitude and temperature variation of  $E_A(T)$ , the mean barriers and 'unphysical' small switching times of the particles are explained. Below  $T_b$  hysteresis loops appear and are quantitatively described by a blocking model, which also ignores particle interactions, but takes the size distributions and the conventional field dependence of  $E_A$  into account.

PACS numbers: 75.50.Tt, 75.40.Gb, 75.75.+a, 75.60.Ej

## I. INTRODUCTION

The development of ferromagnetic particle suitable for high density storage media constitutes one of the present challenges to nanotechnology. Most recently, the central demands of this application, i. e. a narrow size distribution of nanometer crystals and their arrangement in 2- and also 3-dimensional lattices with controllable inter-particle spacing, have been met through organometallic synthetic approaches followed by the self-assembly technique.<sup>1–4</sup> The first ferromagnetic nanocrystals prepared by this organometallic route were FePt<sup>1</sup> and Co<sup>2</sup> as well, aimed at sufficiently large anisotropy energies at a minimum particle volume  $V_p$ . This should drive the thermal fluctuation time  $\tau=\tau_0 \exp(E_B/k_B T)$  from the microscopic values,  $\tau_0 = 10^{-10} - 10^{-12}$  s,<sup>5</sup> beyond the values necessary for the storage stability.<sup>6</sup> At this point, the physical characterization of the nanoparticles is required to explore and understand the origin and the magnitude of the density of the anisotropy energy,  $K_A \approx E_A/V_p$ , which determines the energy barrier  $E_B \approx E_A$  for coherent rotation of the particle moment  $\mu_p$ . Rather large values of  $K_A \approx 6 \cdot 10^6$  J/m<sup>3</sup> have been achieved for iron-rich Fe<sub>x</sub>Pt<sub>1-x</sub> ( $x \approx 0.52$  to 0.60) nanoparticles after controlled annealing at high temperatures,<sup>1</sup> which transformed the fcc to the face-centered tetragonal L1<sub>0</sub>-structure. Due to the larger spin-orbit coupling of cobalt, Co-based nanoparticles may be expected to provide a higher anisotropy, even

in the as grown state. In fact, very recently, surprisingly large values up to  $2 \cdot 10^6$  J/m<sup>3</sup> have been reported for 1 nm fcc-Co particles and attributed to the enhancement of  $K_A$  at the surface.<sup>7</sup> In addition, Co<sub>x</sub>Pt<sub>1-x</sub> nanoparticles have also been prepared by magnetron sputtering<sup>8</sup> and a microemulsion technique<sup>9</sup> reaching a maximum anisotropy,  $K_A \approx 0.6 \cdot 10^6$  J/m<sup>3</sup> for  $x=0.75$ .<sup>7</sup> Somewhat smaller values were obtained for as grown  $x=0.25$ - and annealed  $x=0.5$ -particles.<sup>8</sup> The sources for these anisotropies could not yet be identified, but, considering more detailed studies on annealed Co<sub>x</sub>Pt<sub>1-x</sub> films,<sup>10</sup> internal grain boundaries separating different structures are the most likely candidates for enhanced anisotropies in addition to surface effects.

In the present work, we present a detailed physical characterization of spherical CoPt<sub>3</sub>-nanocrystals prepared by organometallic route in high boiling coordinating solvents mixtures<sup>3</sup> The possibility to grow 2D and 3D superstructures using the capped particles has been demonstrated by us and the coauthors in Ref. 4. Our study is directed towards a determination of the superparamagnetic behavior and the onset of anisotropy in as grown, single fcc-phase CoPt<sub>3</sub> nanoparticles. This is intended to provide a deeper insight into the nature of the magnetic blocking of the single-phase, and interaction-free nanocrystals, i. e. in the transition from superpara(SPM)- to superferromagnetism(SFM). In the seminal work by Bean and Livingstone,<sup>11</sup> this dynamical crossover has been defined to occur at the so-called

blocking temperature,  $T_b \cong E_B/25 k_B$ , where remanent magnetizations and coercivity appear. For the first time, we also examine the effects of  $E_A$  on the low-field *equilibrium* magnetization  $M(H,T)$ , i. e. at temperatures distinctly above  $T_b$ . To this end, we apply a recent general framework by Garcia-Palacios<sup>12</sup> and take into account the anisotropy in the statistical evaluation of the magnetization for particles assemblies with randomly distributed anisotropy axes. It turns out that, starting from the isotropic behavior at zero magnetic field  $H$ , the magnetization isotherms  $M(H,T)$  fall progressively below the commonly supposed Langevin-function  $\mathcal{L}(\mu_p H/k_B T)$  due to the presence of a finite anisotropy field as defined in Ref. 11,  $H_A = 2E_A/\mu_p$ . We believe, that for large anisotropies, the evaluation of  $E_A$  from the 'low-field' isotherms is advantageous over the frequently used asymptotic law,  $M(H,T) \cong M_0[\mathcal{L}(x) - \frac{1}{15}(H_A/H)^2]$  (see e. g. Ref. 13,14), because the validity of the latter requires rather high fields,  $H \gg H_A$ , which is difficult to reach for strong anisotropy. Moreover, additional paramagnetic contributions from unavoidable impurity phases in the nanoparticle assemblies and also from the Langevin-function  $\mathcal{L}(x)$  may interfere in high fields.<sup>14</sup> We hope, that our analyses will not only contribute to solving this general problem, but that the results will also provide a basis for a further modification of CoPt<sub>3</sub>-nanocrystals in order to optimize the anisotropy.

The outline of this paper is the following. In Section II, the structural features of the two nanoparticle assemblies under investigation and the magnetic measurements are described. In Section III, at first the results of the temperature-dependent DC-susceptibilities are analyzed to extract the temperature variation of the particle spontaneous magnetization, the blocking temperatures, and the effects of the narrow particle size distributions on the blocking behavior of the zero-field cooled susceptibility  $\chi_{ZFC}$ . Then we present AC-susceptibilities, from which the mean thermal activation barriers,  $E_m$ , and their distribution functions are determined. These latter are compared with the results from  $\chi_{ZFC}$  and the TEM images as well. In Section IV, we report on magnetization isotherms recorded between 5 K and 350 K. At first, from the Langevin behavior observed at high temperatures the mean magnetic moments of the particles  $\mu_p$  and per CoPt<sub>3</sub> are deduced. Then, approaching the blocking temperatures from above, the increasing effect of a temperature dependent anisotropy is observed and evaluated. The extrapolation of the resulting  $E_A(T)$  to  $T=0$  yields energies consistent with the barriers from the AC-susceptibilities and yields an energy density of  $K_A=0.12 \cdot 10^6 \text{ J/m}^3$  independent of the nanoparticle volume. Finally, the hysteresis loops in the SFM regime,  $T < T_b$ , are presented and analyzed based on the particle size distributions and the anisotropic SPM magnetization. Section V closes the work with the conclusions.

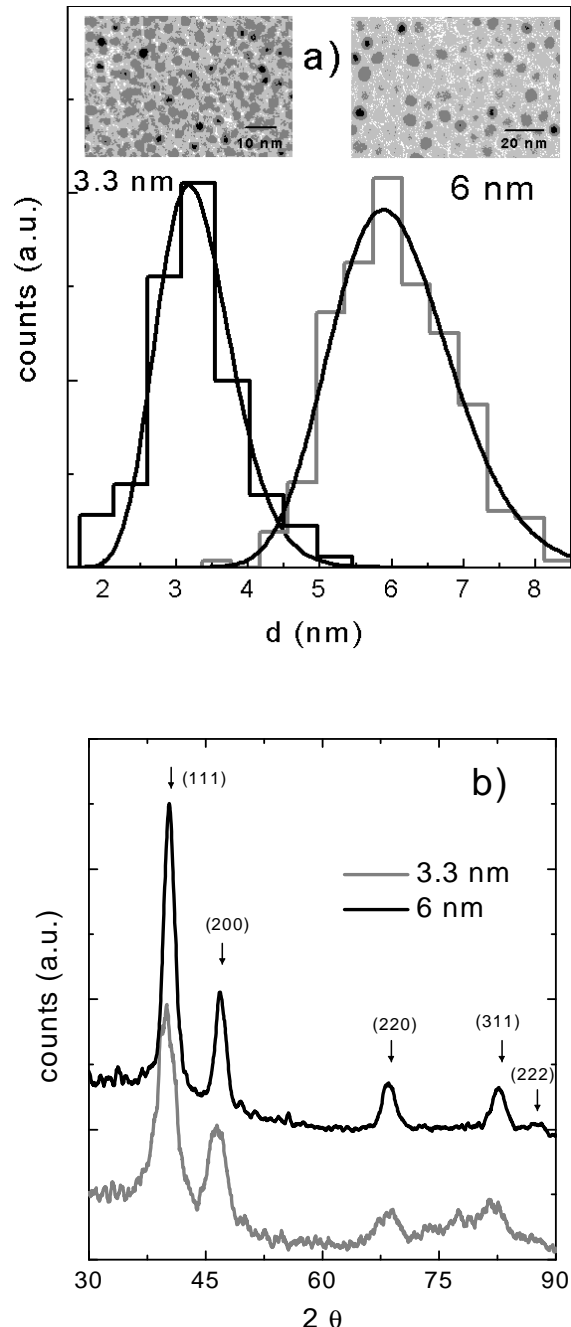


FIG. 1: a) Distribution histograms for particle diameters in CoPt<sub>3</sub> nanocrystal-powders determined from TEM-pictures, clips of which are displayed by the insets; solid curves represent distribution functions discussed in the text. b) XRD wide-angle scans, which evidence the fcc-structure.

## II. EXPERIMENTAL

The organometallic route, by which the present assemblies of size-selected capped particle were prepared, has been described in some detail in Ref. 4. The Co:Pt=1:3 composition of the final products has been checked by energy dispersive absorption of  $\chi$ -rays. Wide angle

X-ray diffraction (XRD) scans, recorded on the pure nanocrystalline powders using  $CuK\alpha$ -radiation (Philips X-pert) are shown in Fig. 1(a). The XRD and an inspection of TEM-images clearly reveal particles with a single crystalline fcc-phase with lattice constant  $a_0 = 3.86 \text{ \AA}$ , in agreement with the bulk value.<sup>15</sup> Transmission electron microscopy (TEM) images of both particle assemblies and their analyses are depicted in Fig. 1(b). The results indicate rather narrow distributions, which can be nicely fitted to the frequently observed log-normal function,  $P(d) = (\sqrt{2\pi}\sigma_d d)^{-1} \exp(-\ln^2(d/d_m)/2\sigma_d^2)$ . One finds rather narrow widths,  $\sigma_d=0.16$  and  $\sigma_d=0.14$  and for the particle diameters  $d_p = \exp(\sigma_d^2/2)d_m = 3.3 \text{ nm}$  and  $6.0 \text{ nm}$ , see Table I below. All magnetic measurements, i. e. the temperature variation of the low-field magnetizations and also the field sweeps up to 10 kOe at fixed temperatures between 5 K and 400 K have been performed using a SQUID-magnetometer (QUANTUM DESIGN, MPMS 2). By an AC-option we investigated the dynamic susceptibility,  $\chi' - i\chi''$ , between 0.1 Hz and 1 kHz at  $H=0$ , where the excitation amplitude was kept small enough in order to detect the linear response. As an optimum sensivity we reached  $\sigma_{rms} \approx 10^{-8} \text{ emu}$ .

### III. ZERO-FIELD SUSCEPTIBILITIES

#### A. DC-Limit

The temperature dependence of the DC-susceptibilities has been determined from the magnetizations measured in a weak field of 100 Oe which is weak enough to provide the zero-field limit. The only exceptions occur at a few low temperatures for the CoPt<sub>3</sub>-6 sample, but there the finite field can easily be taken into account in the evaluation. The insets to Fig. 2 show that the susceptibilities display a reversible behavior down to the blocking temperatures  $T_b$ , (listed in Table I), where the zero-field cooled (ZFC) and field-cooled (FC) become different. Also at  $T_b$ , the remanent magnetization (REM), measured at increasing temperature after the FC-run and subsequent removal of the field, disappears, see the inset to Fig. 2(a). There, as an interesting effect a kind of sum-rule appears,  $M_{FC} \approx M_{ZFC} + M_{REM}$ , which implies that the blocked and the remanent parts of the total (FC) magnetization are identical within the measuring time. The blocking temperatures themselves allow a first estimate of the mean energy barriers of the nanoparticles against coherent rotation of  $\vec{\mu}_p$ . Using the classical estimate,  $E_B \cong 25 k_B T_b$ ,<sup>11</sup> yields values of about 950 K and 200 K, which roughly scale with the particle volume. This indicates that surface anisotropy plays no role.

A more detailed insight into the blocking process and also into the magnetism above  $T_b$  is given by the effective Curie-constants, depicted in the main frames of Fig. 2 for both powders. This quantity clearly shows (i) the gradual transition from the SPM to the SFM state when

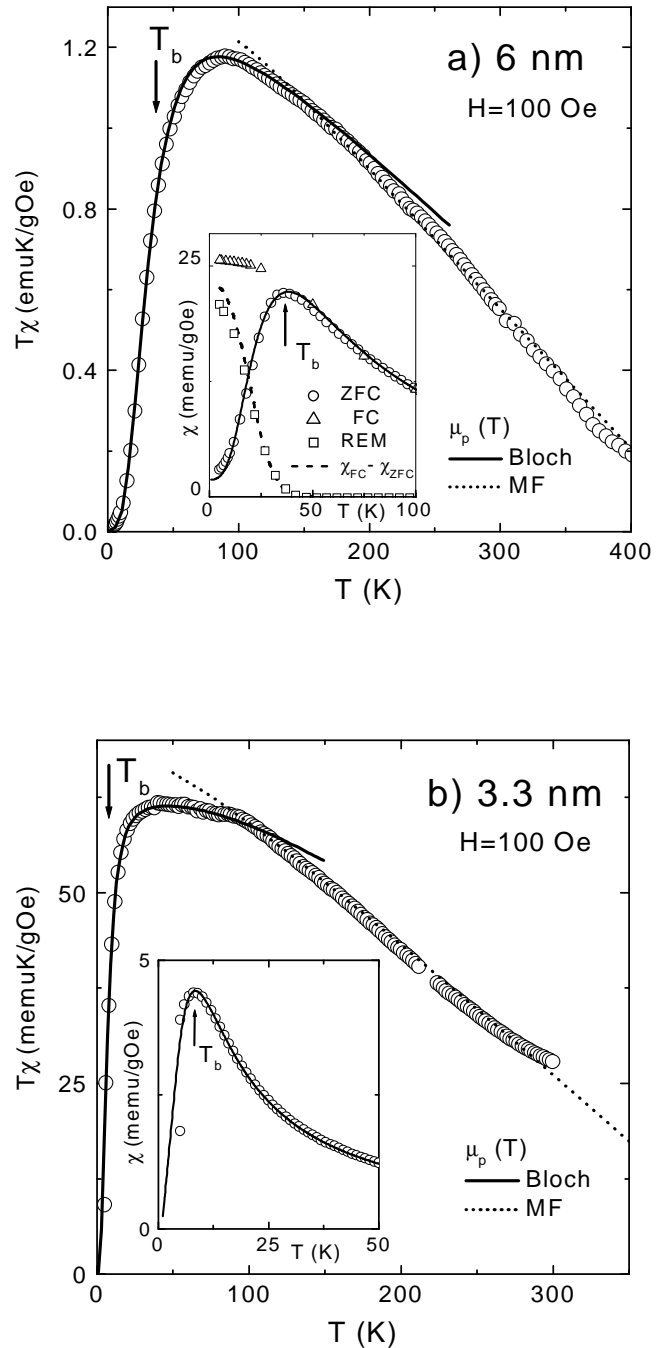


FIG. 2: Temperature dependence of the effective Curie-constants  $\chi T$  of the low-field susceptibilities  $\chi = M/H$  (insets) for the nanoparticle powders a) CoPt-6 and b) CoPt-3. Note that for large  $T$ , the  $\chi T$  extrapolate to the same mean-field Curie-temperature,  $T_{MF} = 450(20) \text{ K}$ . The low temperature regime is dominated by a progressive blocking of particles being described by Eq. 1 using the log-normal distributions inferred from Fig. 1(b). The solid curves in the insets are calculations from Eq. 1 using Bloch's law,  $\mu_p(0)(1 - BT^{3/2})$ , for the moments at low temperatures.

TABLE I: Parameters of the two nanoparticle assemblies determined from the analyses described in the text.

sample	d(nm)	$\sigma_d$	$V_p$ (nm <sup>3</sup> )	$T_b$ (K)	$E_m(0)$ (K)	$\tau_0$ (s <sup>-1</sup> )	$N_p$ (g <sup>-1</sup> )	$\mu_p(0)(\mu_B)$	$\mu_{\text{CoPt}_3}(\mu_B)$	$E_A(0)$ (K)	$K_A(\frac{10^6\text{J}}{\text{m}^3})$
CoPt <sub>3</sub> -3	3.3	0.16	18.8	8.3	178	$2 \cdot 10^{-13}$	$4 \cdot 10^{17}$	785	2.4	125	0.11
CoPt <sub>3</sub> -6	6.0	0.14	131	37.5	990	$1.6 \cdot 10^{-15}$	$2 \cdot 10^{17}$	5120	2.5	770	0.10

$T_b$  is passed from above and (ii) a linear decay of  $\chi \cdot T$  towards higher temperatures in the SPM phase, reaching zero at  $T_c=450(10)$  K for both samples (see dotted lines in Fig. 2). This latter feature is easily explained by observing that  $T\chi_{SPM}(T) = \mu_p^2(T)/3k_B\mu_0V_p\rho$  ( $\rho$ =mass density) and assuming that the spontaneous particle moments display a mean-field (MF) like behavior,  $\mu_p(T) = \mu_p(0)(1 - T/T_c)^{1/2}$ . It may be interesting to note, that such a MF-law for  $\mu_p(T)$  was realized in recent Monte Carlo simulations by Altbir et al.<sup>16</sup> for nanosized Co-particles. Our value for  $T_c$  is consistent with 'onset'-temperatures for ferromagnetism of CoPt<sub>3</sub>-films grown on substrate temperatures below 200° C,<sup>15</sup> which is comparable to 300° C where the present nanoparticles were synthesized.<sup>4</sup> On the other hand, the present critical temperature is 150 K larger than  $T_c \approx 300$  K reported for bulk CoPt<sub>3</sub>.<sup>15</sup> The reason for this large difference is not yet known.

At low temperatures,  $T \leq 130$  K, the MF-law becomes invalid, as can be seen most clearly on CoPt<sub>3</sub>-3, where the reduction of  $\chi \cdot T$  by blocking does not interfere with the deviation from MF. Previous analyses of  $\mu_p(T)$  for iron nanocrystals at low temperatures yielded Bloch's law  $\mu_p(T) = \mu_p(0)(1 - BT^{3/2})$ ,<sup>17,18</sup> where the coefficient of 3 nm-particles  $B=1.0 \cdot 10^{-4} K^{-3/2}$  turned out to be more than two orders of magnitude larger than in the bulk,  $3.0 \cdot 10^{-6} K^{-3/2}$ .<sup>18</sup> By fitting our data for  $\mu_p(T \rightarrow 0)$  to this form, we find  $B=0.8 \cdot 10^{-4} K^{-3/2}$ , i. e. a similar large number. An enhancement of the Bloch-coefficient for nanoparticles was also found by MC-simulations in the Heisenberg-model.<sup>19</sup>

Approaching the blocking temperature  $T_b$ , one realizes from  $\chi \cdot T$  that, due to the size distribution of the particles, the larger of them remain blocked up to temperatures above  $T_b$ . Following Wohlfarth<sup>20</sup> and Hansen and Mørup,<sup>21</sup> we describe the blocking effect on the ZFC susceptibility by the expression

$$\chi_{ZFC} \cdot T = C(T) \left[ \int_0^{v_T} dv P(v)v + \int_{v_T}^{\infty} dv P(v)v_T \right] + C_{bgd}, \quad (1)$$

where  $P(v)$  are the distribution functions of the normalized particle volumes  $v = V/V_m$ . Here  $V_m$  defines the maximum of  $P(v)$ . In this approach, the first term accounts for the free rotation of the unblocked smaller moments, while the second one describes the rotations of the blocked (larger) moments within the energy minima produced by their own anisotropy energy  $K_A$ . Of course, dividing the particles into two groups using a single, thermal activation volume  $v_T = V_T/V_m$  is a rather rough approximation and, therefore, we allow  $v_T$  to deviate from

the traditional value  $T/T_b$ <sup>21</sup> by introducing  $v_T = T/T_0$  with the  $T_0 \neq T_b$ . The final term in Eq. 1 accounts for dia- and paramagnetic background susceptibilities, which are small and not of interest here.

The full curves in Fig. 2 have been obtained from fits to Eq. 1 by assuming the log-normal volume distributions  $P(v) = \exp(-\ln^2 v / 2\sigma_v^2) / \sqrt{2\pi}v$  suggested by the TEM images in Fig. 1(b). The fits are rather sensitive to the  $P(v)$ -shape as well as to the widths, yielding  $\sigma_v = 0.60$  and 0.52 for the 6 nm and 3.3 nm particles, respectively. These standard deviations are only slightly larger than those following from the diameter histograms,  $\sigma_v = 3\sigma_d$  (see Table I). For both particles sizes, the fitted thermal blocking volumes  $v_T$  yield  $T_0 = 0.63(5)T_b$ , which implies that Eq. 1 defines blocking temperatures  $T_0$  significantly below the maximum of  $\chi_{ZFC}$  at  $T_b$ . This shift can be easily explained by calculating  $T_b$  from  $d\chi_{ZFC}/dT = 0$ . Using Eq. 1, one finds for the ratio  $v_b = T_b/T_0$  the equation

$$v_b = \int_0^{v_b} dv P(v)v / \int_0^{v_b} dv P(v),$$

which can be solved numerically for  $v_b$ . Inserting the fitted standard deviations we obtain for the classical blocking temperature  $T_b \approx 1.35 T_0$ , being close to the observed value. A small remaining difference is due to the fact that we ignored some temperature variation of the anisotropy energy to be elucidated in Section III. B.

## B. AC-susceptibility

In order to examine the dynamics of the blocking process in some more detail, we have measured the temperature variation of  $\chi(\omega, T)$  at fixed frequencies between 0.1 Hz and 1 kHz. Having discussed the contributions to the total susceptibility in III. A, we focus here on the part which relaxes within the measuring period,  $2\pi/\omega$ , and is observed directly by the loss component  $\chi''(\omega, T)$ . According to Fig. 3 (inset),  $\chi''$  exhibits well-defined maxima at temperatures  $T_\omega$  which upon increasing frequency shift to larger values, as it is typical for a rapid, e. g. Arrhenius-like form of the relaxation time of the particles,  $\tau(T) = \tau_0 \exp(E_m/k_B T)$ .<sup>5</sup> Then the relaxation time at  $T_\omega$  follows from  $\omega\tau(T_\omega)=1$  and plotting  $1/T_\omega$  against  $\log(\omega/2\pi)$  in Fig. 3, we obtain straight lines consistent with Arrhenius' law. Note that such analysis only provides the activation energy at  $T=0$ , while possible temperature variations of  $E_m$  are absorbed by the amplitude  $\tau_0$ . The rather small, microscopic switching

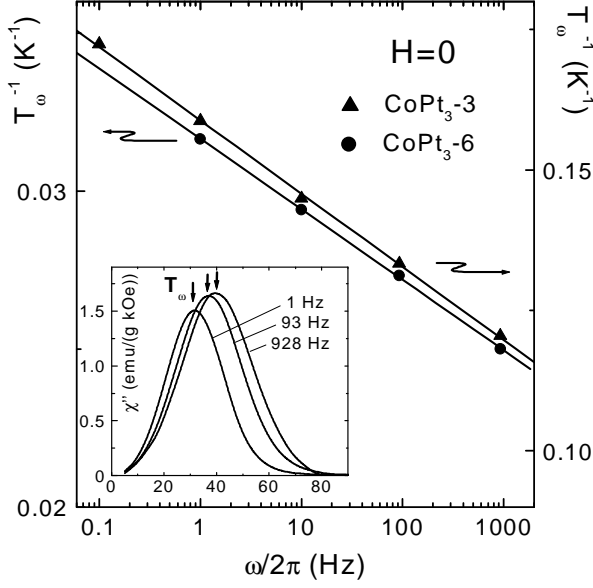


FIG. 3: Arrhenius plots of the peak temperatures  $T_\omega$  of the zero-field magnetic absorption curves  $\chi''(T, \omega)$ , illustrated by the inset. The straight lines are fits providing the energy barriers  $E_B$  at  $T = 0$  and the attempt frequencies  $f_0 = (2\pi\tau_0)^{-1}$  (see Table I).

times of  $\tau_0 = 2 \cdot 10^{-13}$  s and  $2 \cdot 10^{-15}$  s will be discussed in Section V. As for the blocking temperatures, the results for  $E_m$  (Table I) also scale quite nicely with the mean particle volumes  $V_m$  and thus indicate the presence of a volume anisotropy. Relating these barriers to the corresponding blocking temperatures, one finds for the ratios  $E_m/k_B T_b = 24.9$  and  $27.5$  for the 3.3 nm and 6 nm assemblies, which are very close to the classical estimate of 25.<sup>11</sup>

For a further insight into the dynamics of the particle assemblies, we also analyse the shape of  $\chi''(\omega, T)$ . We start with a general ansatz, proposed by Shliomis and Stepanov<sup>22</sup> and applied to experiments by Svedlindh et al.<sup>23</sup> For non-interacting particles, the anisotropy axes of which enclose random oriented angles with the probing AC-field, we can write the ansatz as,<sup>23</sup>

$$\chi(T, \omega) = \frac{C(T)}{T} \int_0^\infty d\epsilon P(\epsilon) \epsilon \times \left\{ \frac{R'/R}{1 + i\omega\tau(\epsilon)} + \frac{1 - R'/R}{1 + i\omega\tau_\perp} \right\} + \chi_{bgd}, \quad (2)$$

where  $P(\epsilon)$  accounts for the distribution  $P(\epsilon)$  of the barriers,  $E = \epsilon E_m$ , against a coherent rotation of the particle moments  $\vec{\mu}$ . Similar as for the ZFC-susceptibility, Eq. 1,  $\chi(T, \omega)$  consists of a longitudinal and a transverse

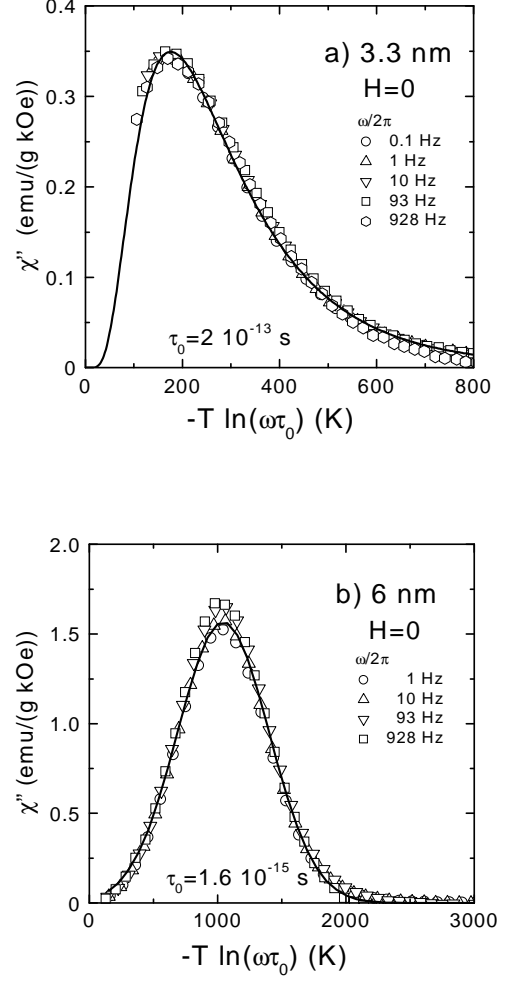


FIG. 4: The magnetic absorption of both powders *versus* scaled temperatures; solid curves represent the 'best' distribution functions for the activations energies, i. e. a) log-normal for CoPt-3 and b) gaussian for CoPt-6.

part describing the inter- and intravalley dynamics of the particles. The relative weights of both contributions are determined by the actual anisotropy  $E$  of a particle via the statistical factors  $R(\sigma) = \int_0^1 dz \exp(\sigma z^2)$  and  $R' = dR/d\sigma$ , where  $\sigma = E/k_B T$ . Since the relaxation time of the (transverse) intravalley motion  $\tau_\perp \approx \tau_0$  is much shorter than the (longitudinal) overbarrier time of the nanoparticles,  $\tau(\epsilon) = \tau_0 \exp(\epsilon E_m/k_B T)$ , the second term will not contribute to the absorption in the present range of frequencies. Moreover,  $\tau(\epsilon)$  varies rapidly as compared to  $\epsilon P(\epsilon)$ , so one can safely substitute under the integral for  $\chi''(\omega, T)$  in Eq. 2,  $\omega\tau/(1 + (\omega\tau)^2) \approx$

$\frac{\pi}{2} k_B T \cdot \delta(\epsilon - \epsilon_\omega)$ ,<sup>12</sup> to yield:

$$\chi''(\omega, T) = \frac{\pi}{2} \frac{k_B C(T)}{E_B} \frac{R'(\epsilon_\omega)}{R(\epsilon_\omega)} P(\epsilon_\omega) \epsilon_\omega. \quad (3)$$

Here,  $\epsilon_\omega = T/T_\omega$  designates the maximum relative barrier, over which a particle can thermally jump within the given observation time  $2\pi/\omega$ , i. e.  $\epsilon_\omega = k_B T(-\ln \omega \tau_0)/E_m$ . Therefore,  $\epsilon_\omega$  is the analogue to  $\epsilon_b$ , with  $-\ln \tau_0/t_b = 25$  used before in the discussion of the ZFC susceptibilities. In the present approximation, the absorption  $\chi''$  just picks up this 'dynamical' fraction  $P(\epsilon_\omega)d\epsilon$  of the distribution. Except for  $P(\epsilon_\omega)$ , the other factors in Eq. 1 vary only little as compared to the distribution function. This includes the ratio  $R'(\epsilon_\omega)/R(\epsilon_\omega)$ , which for  $E_m/k_B T_\omega \approx -\ln \omega \tau_0 \gg 1$  is always close to one,  $R'/R = 1 - k_B T_\omega/E_m$ .<sup>12</sup> Hence, in a plot of  $\chi''(\omega, T)$  vs. the scaled temperature  $-T \ln \omega \tau_0 = \epsilon_\omega E_m/k_B$  all data should collapse on a single curve. According to Eq. 3, this provides the distribution functions for the energy barriers.

The validity of this scaling is demonstrated by Fig. 4 for both nanoparticle assemblies. In the case of CoPt<sub>3</sub>-3 they clearly reveal the same log-normal distribution which already has been obtained from the fit of  $T\chi_{ZFC}$  in Fig. 2(b). There we found a slightly smaller width of the volume distribution than here,  $\sigma_E \approx 0.6$ , for the barriers, which implies for the average barrier  $E_B = E_m \exp(\sigma^2/2) = 195$  K, see Table I). For CoPt<sub>3</sub>-6 a larger difference occurs between the 'volume' distribution functions  $P(v)$ , as obtained from TEM and  $\chi_{ZFC}(T)$  on the one hand, and  $P(\epsilon)$  from the scaling of  $\chi''(\omega, T)$  in Fig. 4(b) on the other hand. The latter unambiguously reveals a gaussian function for the energy distribution with  $E_B = E_m$  (Table I). Although one cannot *a priori* expect that the volume and energy distributions agree, the origin for this change is not clear. It may be interesting to note, however, that very recently the same change, i. e. from log-normal to gaussian energy distributions, has been detected in magnetic noise spectra, in going from 3 nm to 5 nm Co-particles.<sup>24</sup> Let us also note, that the amplitudes of the scaled absorptions in Fig. 4 agree *quantitatively* with those predicted by Eq. 3, if the known Curie-constants  $C(T)$  and mean barriers  $E_B$  are inserted. We consider this a confirmation of the validity of the present model.

#### IV. MAGNETIZATION ISOTHERMS

##### A. Isotropic Superparamagnetism

The field-dependent magnetization curves  $M(H, T)$ , recorded above the zero-field blocking temperatures  $T_b$  of both samples, are anhysteretic, i. e. reversible. There our main objective is to determine the mean magnetic moments of the nanocrystals  $\mu_p$  and to investigate the effects of the anisotropy energy  $E_A$  on  $M(H, T)$ . For not

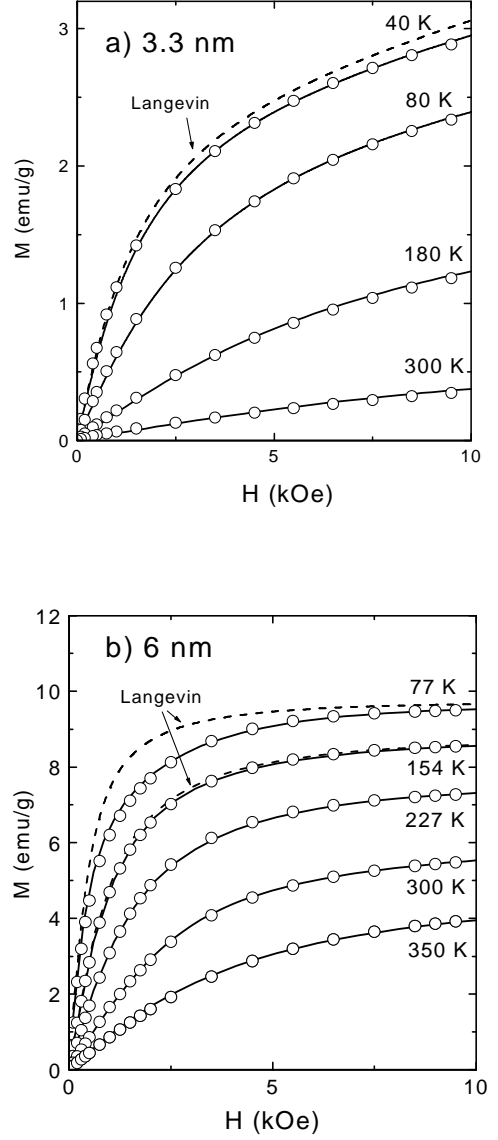


FIG. 5: Magnetization isotherms recorded above the blocking temperatures  $T_b$  of the a) CoPt-3 and b) CoPt-6 samples. The solid lines are fits to Eq. 5 taking into account a finite anisotropy energy,  $E_A(T)$ , describing the significant differences from Langevin-behavior (dotted lines) at low temperatures.

too large  $E_A \leq k_B T$ , the influence on the magnetization is small, so that the traditional analysis based on the Langevin-function,  $\mathcal{L}(x) = 1/\tanh(x) - 1/x$ , represents a good approximation to evaluate  $\mu_p = x \cdot k_B T/H$  from the magnetization isotherms using

$$M(H, T) = N_p \int_0^\infty dv P(v) \mu_p \mathcal{L}\left(\frac{v \mu_p H}{k_B T}\right). \quad (4)$$

Our results for  $M(H, T)$  are shown in Fig. 5 at selected temperatures above  $T_b$ . In fact, for temperatures above  $\sim 200$  K the isotherms can be well described by

the Langevin model, i. e. neglecting any anisotropy, if one uses the MF-type temperature variation of the moments  $\mu_p(T) \sim (T_c - T)^{1/2}$  as indicated by the DC-susceptibility. The most interesting quantities emerging from these fits are the maximum particle moments  $\mu_p(0)$  which, due to the crossover from the MF- to the Bloch-like temperature variation of  $\mu_p(T)$  near  $\approx 130$  K, becomes somewhat smaller than those following from the amplitude of the MF-law for  $\mu_p(T)$ . The results for  $\mu_p(0)$  and the particle densities  $N_p$  are listed in Table I and can be applied to determine the moments per CoPt<sub>3</sub> using the fcc-particle volume of  $57\text{\AA}^3$  in the fcc-structures. We find  $2.4 \mu_B$  and  $2.5 \mu_B$  for the 3.3 nm- and 6 nm-particles being rather close to each other, so that surface effects seem to play no role. These moments are rather close to the bulk values of  $2.42 \mu_B$  determined by neutron scattering<sup>25</sup> and  $2.6 \mu_B$  following from the saturation magnetization measured in fields up to 330 kOe.<sup>15</sup> All these results turn out to be smaller than  $\approx 2.73 \mu_B$ <sup>26</sup> obtained from band structure calculations for CoPt<sub>3</sub>, which predict  $1.86 \mu_B$  for Co and  $0.29 \mu_B$  for each Pt. Such high moments have been reported for CoPt<sub>3</sub> films<sup>10</sup> grown at some elevated temperature,  $T_s = 400^\circ\text{C}$ , which also produced a strongly enhanced anisotropy,  $0.6 \cdot 10^6 \text{ J/m}^3$  at 300 K. At lower deposition temperatures,  $T_s \leq 200$  K, the moments of the films decreased to  $2.2 \mu_B$ , while the anisotropy vanished at 300 K. These remarkable effects were related to the formation of fine Co-platelets in the films.

The mean particle density  $N_p$  obtained for both assemblies and the measured bulk density  $\rho = 3.5 \text{ g/cm}^{-3}$  can be used to evaluate a mean distance between the particles  $D_{nn} \approx (N_p \cdot \rho)^{1/3}$  and, hence, the effect of their dipole-dipole interaction. The strongest effect is expected for the 6 nm particles, where we find  $D_{nn} \cong 12 \text{ nm}$  and  $E_{dd} = \mu_p^2 / 4\pi\mu_0 D_{nn}^3 = 8.5 k_B K$ , while for the 3.3 nm particles  $E_{dd}/k_B = 0.5 \text{ K}$ , turns out to be negligible at all temperatures of interest here,  $T \geq 5 \text{ K}$ . These features justify proceeding with the *pure* interaction-free models.

## B. Anisotropic Superparamagnetism

Upon decreasing the temperature but still above  $T_b$ , the magnetization isotherms begin to fall below the Langevin-shape, which we now try to attribute to the onset of anisotropy. In order to facilitate the computations, we assume here an uniaxial anisotropy, as it is done in most of the literature discussing the dynamical SPM→SFM crossover at  $T_b$ . For randomly distributed axes the influence of anisotropy appears only in finite fields while in zero field the anisotropy effects cancel.

We start with the Hamiltonian of a single anisotropic nanoparticle in a magnetic field  $\vec{H}$ ,

$$\mathcal{H} = -E_A \cos^2 \theta - \vec{\mu}_p \cdot \vec{H},$$

and use the coordinate system displayed in Fig. 6 to calculate the partition function of a particle with the volume

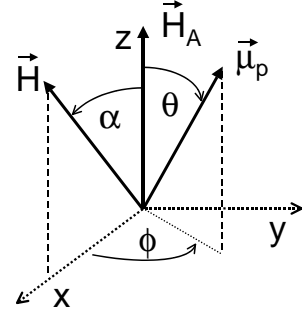


FIG. 6: Definitions of the angles used in the calculation of the magnetization in the anisotropic superparamagnetic regime.

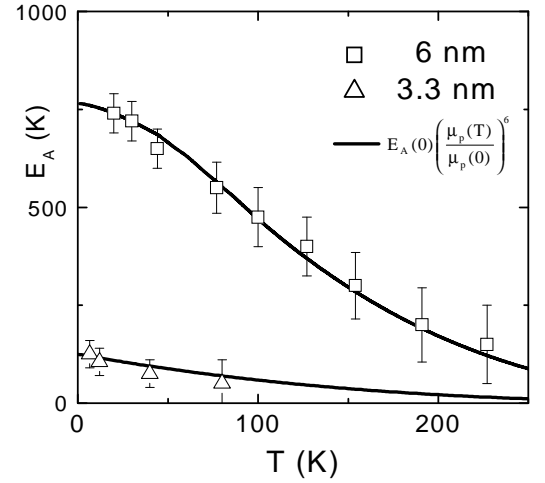


FIG. 7: Temperature variations of the anisotropy energies resulting from the fits to the reversible magnetization isotherms in Fig. 5. The solid curves describe the temperature variations of  $E_A(T)$  in terms of the sixth power of the (spontaneous) particle moments,  $\mu_p(T)$ .

$$V = vV_m:$$

$$Z(H, T, \alpha, v) = \int_{-\pi}^0 d(\cos \theta) \times \exp \left[ \frac{v(E_A \cos^2 \theta + \mu_m H \cos \alpha \cos \theta)}{k_B T} \right] \times I_0 \left( \frac{v \mu_m H \sin \alpha \sin \theta}{k_B T} \right). \quad (5)$$

Here  $I_0(y) = \pi^{-1} \int_0^\pi dt \exp(y \cos t)$  represents the modified Bessel-function to order zero, resulting from the integration over the spherical coordinate  $\phi$ . Then the magnetization of  $N_p$  particles per gram with a random

orientation (in principle, other distributions may be included, but are unlikely here) of the  $\vec{H}_A$  is calculated from standard thermodynamics. After integration over  $\alpha$ , we obtain:

$$M(H, T, v) = N_p k_B T \frac{1}{2} \int_0^\pi d(\cos \alpha) \cdot \frac{\partial \ln Z}{\partial H}. \quad (6)$$

Finally, we use the log-normal distributions for the particle volumes obtained in Section III from the blocking behavior of the DC-susceptibilities, to calculate the magnetization of the present particle assemblies:

$$M(H, T) = \int_0^\infty dv P(v) M(H, T, v). \quad (7)$$

Although these calculations are somewhat time-consuming, depending on the resolution to which the volume-averaging is carried out, their comparison with the data is straightforward. This is due to the fact that the MF- and Bloch-like temperature variations of the particle moments are known, so that the anisotropy energy  $E_A$  is the only parameter to be fitted.

In Fig. 5, the influence of  $E_A$  on both assemblies is shown to become significant at the lowest temperatures. This is demonstrated by a reduction of  $M(H, T)$  to below the isotropic (Langevin) limits indicated by dotted curves. Due to the lower  $E_A$ -values of the 3 nm particles, the effect is smaller there and becomes even weaker at higher temperatures. The physical reason for this reduction is traced to the fact that, under the influence of the increasing field, the particles prefer to stay in states with transverse magnetization. Thus, even for a random distribution of the easy axes,  $M(H, T)$  becomes smaller in comparison to the isotropic (Langevin) case. For a special set of parameters, this effect has been demonstrated by a recent calculation.<sup>12</sup>

Although the increasing thermal fluctuations tend to drive the magnetization towards Langevin behavior, it is possible to extract  $E_A(T)$  from our fits of the equilibrium magnetizations to Eq. 5. The results for  $E_A(T)$  are depicted in Fig. 7, showing that the anisotropy itself decreases with temperature. Like the energy barriers  $E_B$ , determined from the dynamic behavior in Section III, the anisotropy scales with the mean particle volumes  $V_p$ , and may therefore also be associated with the bulk CoPt<sub>3</sub> phase. In order to discuss the temperature variation of the anisotropy, we relate it to the particle magnetization by the conventional power law,  $E_A(T) = E_A(0)(\mu_p(T)/\mu_p(0))^n$ . The corresponding best fits yield  $n \sim 6$  and are indicated in Fig. 7. We do not know of any theoretical predictions for the temperature variation of  $E_A$  in nanoparticles, to which this result can be compared. As a remarkable feature, however, we should mention, that the amplitudes  $E_A(0) \approx 145$  K and 800 K are close to the energy barriers  $E_B$  determined in Section III at low temperatures from the blocking and the

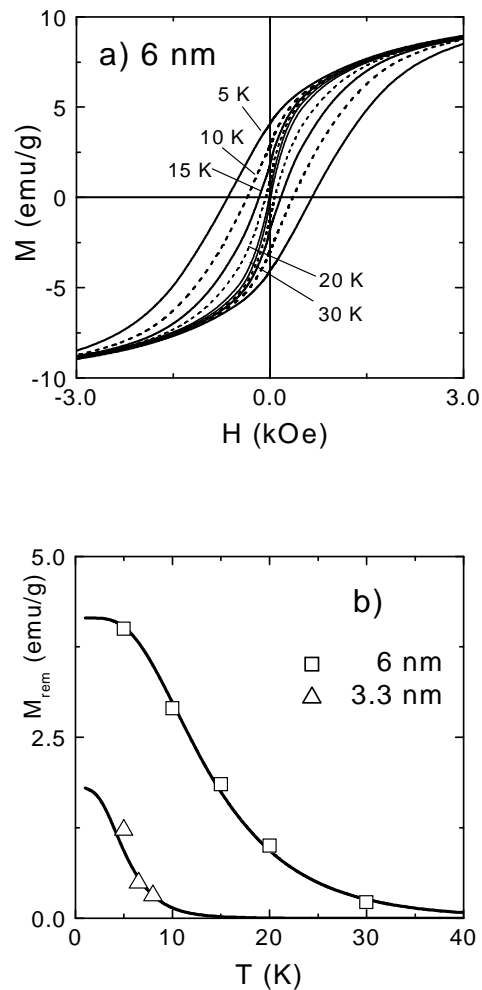


FIG. 8: a) Hysteresis loops measured below the blocking temperature  $T_b$  of 6 nm CoPt<sub>3</sub>-nanoparticles. b) Temperature variation of the remanent magnetizations, the solid curves are fits to Eq. 7.

finite dissipation  $\sim \chi''$ . Using the mean particle volumes, we find a mean density for the anisotropy energy of  $0.10(2) \cdot 10^6$  J/m<sup>3</sup>. Whether this value can be enhanced by annealing and a possible generation of Co-rich platelets as in Ref. 10 remains a challenge for the future preparation.

### C. Superferromagnetic regime

We now enter the temperature regime below  $T_b$  which is characterized by the appearance of hysteresis in the magnetization isotherms, as illustrated by Fig. 8(a) for the 6 nm particles. Except for the lowest temperatures of 5 K we can discuss all results without taking particle-particle interactions into account. This SFM behavior is in contrast to the interacting case, where below some col-



lective ordering temperature spin-glass or -at larger particle densities- long-range ferromagnetism may appear.

Let us start with the remanent magnetizations measured after sweeps to a maximum field of 10 kOe and shown in Fig. 8(b) for both samples. Within the SFM model of independent particles the most obvious ansatz to describe the temperature variation is

$$M_{rem}(T) = M_{rem}(0) \int_{v_T^*}^{\infty} dv P(v). \quad (8)$$

This form ascribes the remanence to arise from particles larger than a thermal activation volume  $v_T^*$ . We assume  $v_T^*$  to be different from the classical limit, Eq. 1, by taking  $v_T^* = T/T_0^*$ . However, as a matter of fact, the best threshold value to fit the data of the 3 nm particles in Fig. 8(b) is  $v_T^* = 0.95v_T$ , i. e. agrees well with  $v_T$  derived from the SPM susceptibility, Eq. 1. For the 6 nm particles we obtain a larger effective  $v_T^* = 1.5v_T$ . This result implies that the thermal blocking volume of the remanent magnetization is by a factor of 1.5 larger than  $v_T$  obtained from the ZFC susceptibility peak, Eq. 1. One could conjecture that the onset of dipolar interactions between the 6 nm-particles may be responsible for this enhancement of  $v_T$ , however, the amplitudes resulting from the fits to Eq. 6, i. e.  $M_{rem}(0) = 1.9$  emu/g and 4.7 emu/g are rather close to 0.5  $M(0)$  (s. Table I). This is fully consistent with the Stoner-Wohlfarth model for interaction-free particles with randomly distributed uniaxial anisotropy axes.

As a further test of this model, we discuss now the field variations of the magnetization below  $T_b$ . To this end, we consider separately the irreversible and reversible contributions,  $M_{irr} = (M_+ - M_-)/2$  and  $M_{rev} = (M_+ + M_-)/2$ , respectively, where  $M_+$  and  $M_-$  denote the branches of the hysteresis loops recorded upon increasing and decreasing magnetic field. The field dependences of  $M_{irr}$  are shown in Fig. 9(a) and 9(b) for both particle assemblies. By extending the analysis of the remanence to finite fields, we try to relate the irreversible magnetization to those particles which still remain to be blocked in the presence of  $H$ :

$$M_{irr}(H, T) = M_{rem}(T) \int_{v_T^*(H)}^{\infty} P(v) dv \quad H < H_{irr}(T). \quad (9)$$

Here  $v_T^*(H) = v_T^*/(1 - H/H_{irr}(T))^\beta$  represents the minimum relative blocking volume. As the best 'simple' exponent to describe the field variation we found  $\beta = 2$ , which was introduced by Bean and Livingstone<sup>11</sup> for the field dependence of the particle anisotropy energy. This exponent produces rather nice fits to Eq. 8 (see Fig. 9(a) and 9(b)) using the amplitude from Eq. 7 so that the effective irreversibility field  $H_{irr}$  is the only free parameter. According to our definition, this characteristic field marks the onset of irreversibility in hysteresis loops. Here we

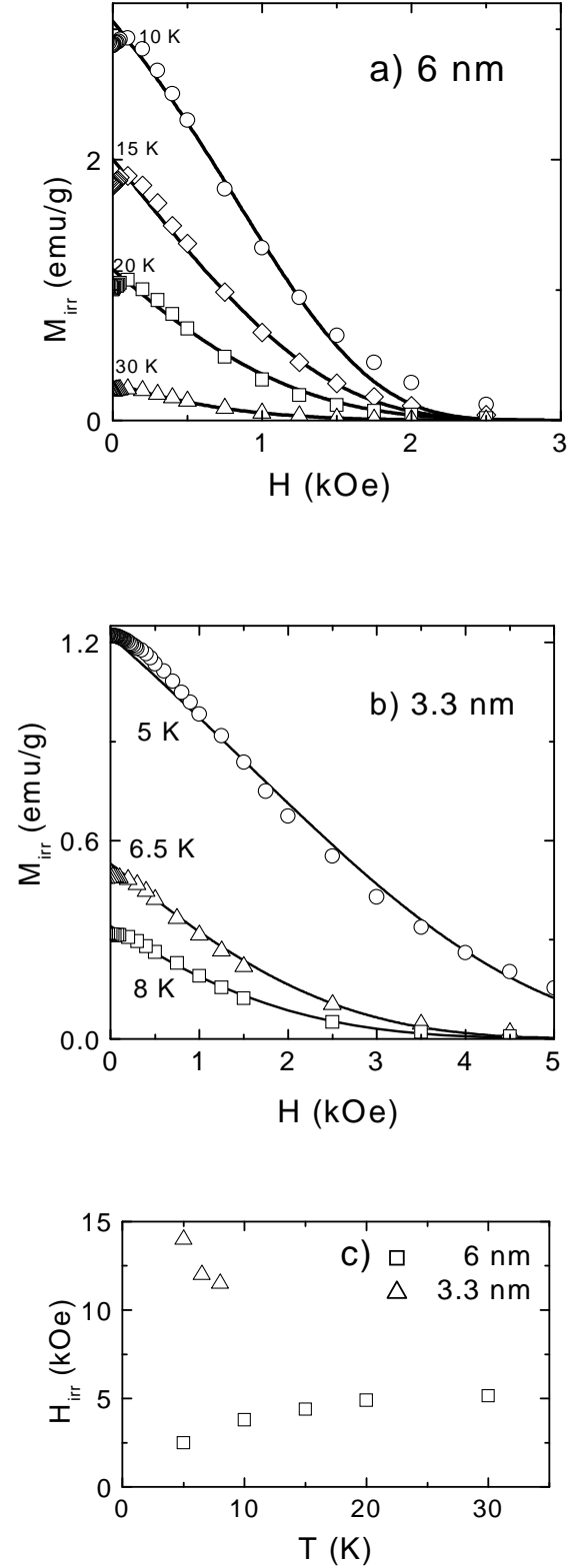


FIG. 9: Irreversible contributions to the hysteresis loops of a) 6 nm (see Fig. 8(a)) and b) 3.3 nm particles. Solid lines are fits according to Eq. 8 ; c) temperature variation of the irreversibility fields following from the fits in a) and b).

should note that  $M_{irr}$  determined for the 6 nm particles at our lowest temperature, 5 K, could no longer be fitted by Eq. 8. Referring to our estimate of particle interactions in Section III. A,  $T_{dd} = 8.5$  K, we may attribute this feature to the onset of collective effects.

The results for  $H_{irr}(T)$  are displayed in Fig. 9(c). As the most interesting feature we regard the fact, that for the 6 nm nanoparticles  $H_{irr}(T)$  agrees almost perfectly with the anisotropy field resulting from the low temperature anisotropy energy. Using the values of Table I, we obtain  $H_A = 2E_A/\mu_p = 4.7$  kOe. For the 3 nm particles the data of Table I yield the same anisotropy field, which qualifies this quantity together with  $K_A$ , as a bulk property. Here, however, the irreversibility field of  $H_{irr} = 13(1)$  kOe turns out to be much larger than  $H_A$ . We tentatively attribute this feature to the much larger paramagnetic background in this sample,  $\chi_p(T) = C_p/(T + 50\text{K})$ . Associating the Curie-constant  $C_p$  with non-crystallized CoPt<sub>3</sub>, we find a fraction of  $\approx 30\%$  of this phase and we suspect that at the present low temperatures the paramagnetic moments are polarized in the local fields of the oriented nanocrystals so that the effective blocking volume and, hence, the irreversibility field is enhanced.

Finally we apply the present model to the reversible magnetizations. In Fig. 10 we have depicted just one low-temperature isotherm for each sample, where the blocking effects are largest. In order to describe the data, we assume that below  $T_b(H)$  only unblocked particles ( $v < v_T^*(H)$ ) contribute to  $M_{rev}$ . They provide the anisotropic SPM magnetization which can be calculated from Eq. 5,

$$M_{rev}(H, T) = \int_0^{v_T^*(H)} dv P(v) M(H, T, v). \quad (10)$$

The results are also indicated in Fig. 10 and show excellent agreement with the data for both nanocrystalline assemblies. Since the same is true for all larger temperatures, we have achieved here a complete description of the hysteretic magnetizations.

## V. CONCLUSIONS

Our investigations of the zero-field DC- and AC- susceptibilities and field dependent magnetizations of two CoPt<sub>3</sub>-nanoparticle assemblies with mean diameters of 3.3 nm and 6 nm provide the first clear evidence for anisotropic superparamagnetism (ASPM). The signature of the ASPM is a *reduced equilibrium* magnetization. On the temperature axis, ASPM appears between the conventional Langevin-type SPM present at large  $T \geq E_A(T)/k_B$ , where thermal fluctuations override the anisotropy, and the so-called superferromagnetism (SFM) occurring below the blocking temperature,  $T_b = E_A(T)/25k_B$ ,<sup>11</sup> which represents a non-equilibrium

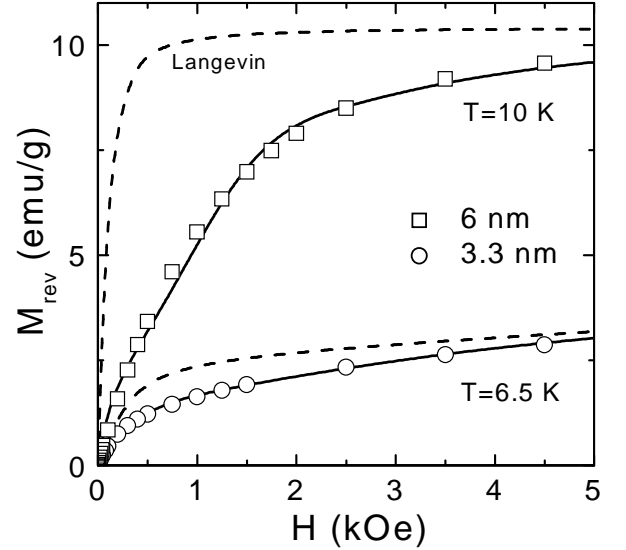


FIG. 10: Reversible part of the hysteresis loops for two low temperatures of both nanoparticle assemblies. Solid lines represent *ab initio* calculations from Eq. 9, using the maximum unblocked volume  $v_T^*(H)$  as determined from the fits of the irreversible magnetizations in Fig. 9. For comparison, the isotropic Langevin-functions for both samples are indicated.

phase depending on the observation time  $t_0$ . The reduction of  $M(T, H)$  in the ASPM regime of nanoparticles with randomly oriented anisotropy axes, appears only in finite magnetic fields  $\vec{H}$ . This effect has recently been predicted<sup>12</sup> to arise from a slightly preferred statistical weight for particles with perpendicular orientation of their preferred axis relative to  $\vec{H}$ .

We have analysed our  $M(H, T)$  curves using the full statistical model and deduced a rather strong temperature and size variation of the (uniaxial) anisotropy  $E_A(T)$ . The linear variation of  $E_A$  with the particle volumes reveals the dominance of a bulk anisotropy density of  $K_A(0) = 1.2 \cdot 10^6$  J/m<sup>3</sup>. Its temperature dependence could be described in terms of the spontaneous particle moments,  $E_A(T) \sim \mu_p^6(T)$ , but the origin of this high power is not yet known. This result implies that anisotropy effects in nanoparticles with rather low Curie-temperatures and moderate  $K_A(0)$ -values, as here for CoPt<sub>3</sub>, become important at lower temperatures. They should receive attention for alloys with enhanced anisotropies, as prepared recently for possible high density storage fabrication.<sup>1,2,6,8</sup> In such materials, of course, the transition to the SFM state at  $T_b$  may be shifted to beyond room temperatures. Below  $T_b$ , we could explain the hysteretic magnetization quantitatively within the ASPM model considering blocking and the particle distribution functions.

Finally, we point out an interesting consequence emerging from the temperature variation of the anisotropy  $E_A(T)$ . This refers to the activation energy  $E_m$  and the time scale  $\tau_0$  of the Arrhenius' law which

is traditionally used to determine the anisotropy  $E_A$  from blocking phenomena, like the magnetic absorption  $\chi''(\omega, T)$  or peaks of  $\chi_{ZFC}(T)$ . Our analyses of  $\chi''$  in Section III. B produced values (i) for  $E_m$ , which were larger than the anisotropy energies, determined in the ASPM regime (s. Fig. 7), and (ii) for  $\tau_0$ , which appeared small and strongly size-dependent (s. Table I). Both features can be understood by considering the fact that high barriers imply a rather narrow temperature range of  $T_\omega$  available for the Arrhenius' analysis, see inset to Fig. 3. Then taking into account the temperature variation of  $E_A$  one may consider it to lowest order as the expansion around some mean temperature  $T_\omega$  from this range:

$$E_A(T) = E_A(T_\omega) + E'_A(T_\omega)(T - T_\omega) + \dots$$

where  $E'_A(T_\omega) = (dE_A/dT)_{T=T_\omega}$ . Inserting this as 'true' barrier into Arrhenius' law  $\tau_0 = \tau_A \exp(E_A(T)/k_B T)$ , one finds the same form  $\tau = \tau_0 \exp(E_m/k_B T)$ , but with renormalized parameters  $E_m = E_A(T_\omega) - E'_A(T_\omega)T_\omega$  and  $\tau_0 = \tau_A \exp(E'_A(T_\omega)/k_B)$ . Since the anisotropy energy generally decreases with temperature, the conventional analysis overestimates the barrier and produces too small switching times. For the present nanoparticles we found  $E_A(T) = E_A(0)(\mu_p(T)/\mu_p(0))^6$ , see Fig. 6, and since the peak temperatures occurred at low temperatures, the Bloch's form,  $\mu_p(T)/\mu_p(0) = 1 - (T/T_0)^{3/2}$  should be employed. Using our results from Section III. A, i. e. the same  $T_0 = B^{-2/3} = 640$  K for both particle

sizes, yields for the 'true' barrier against particle switching  $E_A(T_\omega) = E_m[1 - 9(T_\omega/T_0)^{3/2}]$  and for the real switching time  $\tau_A = \tau_0 \exp[(9E_A(T_\omega)/k_B T_\omega)(T_\omega/T_0)^{3/2}]$ . Note that the MF-type variation of  $\mu_p(T)$  yields much larger corrections. The strongest effect here is expected for the 6 nm particles with  $T_\omega \approx 40$  K, where we obtain  $E_A(T_\omega)/k_B = 850$  K, close to the results from the magnetization isotherms in the ASPM regime, while for 3.3 nm ( $T_\omega \approx 9$  K) the corrections are negligible. For the switching time we obtain  $\tau_A = 1.0 \cdot 10^{-13}$  s, which is close to  $\tau_A = \tau_0 = 2 \cdot 10^{-13}$  s for the 3 nm particles. This suggests a comparison to the prediction by the Néel-Brown theory<sup>5,12,27</sup>  $\tau_N = (\pi k_B T/E_A)^{1/2}(\eta_r + \eta_r^{-1})/2\gamma H_A$ . Since the anisotropy field  $H_A = 4.8$  kOe and also  $\pi k_B T_\omega/E_A \approx 0.1$  turned out to be independent from particle size we find for both assemblies  $\tau_N = (\eta_r + \eta_r^{-1}) \cdot 1.8 \cdot 10^{-12}$  s. Obviously no value of the Landau-Lifschitz-Gilbert parameter  $\eta_r$  can explain the experimental results for  $\tau_A$ . As another, rather rough estimate we assume thermal agitation  $\tau_T = \hbar/k_B T_\omega$ , which leads to more consistent values of  $2 \cdot 10^{-13}$  s and  $8 \cdot 10^{-13}$  s for the 6 nm and 3 nm particles, respectively. In order to shed more light into these microscopic dynamics, we presently investigate the ferromagnetic resonance on the CoPt<sub>3</sub> nanocrystals.<sup>28</sup>

This work is part of the program of the Graduiertenkolleg 'Physics of Nanostructured Solids' financed by special funds of the Deutsche Forschungsgemeinschaft.

- 
- <sup>1</sup> S. Sun, C.B. Murray, D. Weller, L. Folks, and A. Moser, *Science* **287**, 1989 (2000).
  - <sup>2</sup> V.F. Puentes, K.M. Krishnan, and A.P. Alivisatos, *Science* **291**, 2115 (2001).
  - C.B. Murray, S. Sun, W. Gaschler, H. Doyle, T.A. Betley, and C.R. Kagan, *IBM J.Res.& Dev.* **45**, No. 1 (2001).
  - <sup>3</sup> E. V. Shevchenko, D. V. Talapin, A. L. Rogach, A. Kronowski, M. Haase, and H. Weller, *JACS* in press.
  - <sup>4</sup> E. V. Shevchenko, D. V. Talapin, A. Kronowski, F. Wiekhorst, J. Kötzler, M. Haase, A. L. Rogach, and H. Weller, *Adv.Mater.* **14**, 287 (2002).
  - <sup>5</sup> L. Néel, *Ann. Geophys.* **5**, 99 (1949).
  - W.F. Brown, *J.Appl.Phys.* **30**, 130S (1959).
  - <sup>6</sup> D. Weller and A. Moser, *IEEE Trans.Magn.* **35**, 4423 (1999).
  - <sup>7</sup> F. Luis, J.M. Torres, L.M. Garcia, J. Bartolom, J. Stankiewicz, F. Petroff, F. Fettar, J.L. Maurice, and A. Vauris, *Phys.Rev.B* **65**, 094409 (2002).
  - <sup>8</sup> T. Ibusuki, S. Kojima, O. Kitakami, and Y. Shimada, *IEEE Trans.Magn.* **37**, 1295 (2001).
  - <sup>9</sup> A. Kumbhar, L. Spinu, F. Agnoli, K.Y. Wang, W. Zhou, and C.J. O'Connor, *IEEE Trans.Magn.* **37**, 216 (2001).
  - <sup>10</sup> A.L. Shapiro, P.W. Rooney, M.Q. Tran, F. Hellmann, K.M. Ring, K.L. Kavanagh, B. Rellinghaus, and D. Weller, *Phys.Rev.B* **60**, 12826 (1999).
  - <sup>11</sup> C.P. Bean and J.D. Livingston, *J.Appl.Phys.* **30**, 120 S (1959).
  - <sup>12</sup> J.L. Garcia-Palacios, *Adv. Chem. Phys* **112**, 1 (2000).
  - <sup>13</sup> C. Djega-Mariadassou, J.L. Dormann, and M. Nogués, *IEEE Trans. Magn.* **26**, 1819 (1990).
  - <sup>14</sup> M. Respaud, J.M. Broto, H. Rakoto, A.R. Fert, L. Thomas, B. Barbara, M. Verelst, E. Snoeck, P. Lecante, A. Mosset, J. Osuna, T. Ould Ely, C. Amiens, B. Chaudret, *Phys.Rev.B* **57**, 2925 (1998).
  - <sup>15</sup> T.H. Kim, M.C. Cadeville, A. Dinia, and V. Pierron-Bohnes, *Phys.Rev. B* **54**, 3408 (1996).
  - <sup>16</sup> D. Altbir, P. Vargas, and J. d'Albuquerque e Castro, *Phys.Rev.B* **64**, 012410 (2001).
  - P. Vargas, D. Altbir, and J. e Castro, *J.Magn.Magn.Mat.* **226-230**, 603 (2001).
  - <sup>17</sup> G. Xiao and C.L. Chien, *J.Appl.Phys.* **61**, 3308 (1987).
  - <sup>18</sup> D. Zhang, K.J. Klabunde, and C.M. Sorensen, *Phys.Rev.B* **58**, 14167 (1998).
  - <sup>19</sup> P.V. Hendriksen and S. Linderorth, *Phys.Rev.B* **48**, 7259 (1993).
  - <sup>20</sup> E.P. Wohlfarth, *Phys.Lett.A* **70**, 489 (1979).
  - <sup>21</sup> M.F. Hansen and S. Mørup, *J.Magn.Magn.Mat.* **203**, 214 (1999).
  - <sup>22</sup> M.F.Shliomis and V.I. Stepanov, *J.Magn.Magn.Mat.* **122**, 176 (1993).
  - <sup>23</sup> P. Svedlindh, T. Jonsson, and J.L. Garcia-Palacios, *J.Magn.Magn.Mat.* **169**, 323 (1997).
  - <sup>24</sup> S.I. Woods, J.R. Kirtley, S. Sun, and R.H. Koch, *Phys.Rev.Lett.* **87**, 137205 (2001).
  - <sup>25</sup> F. Menzinger and A. Paoletti, *Phys.Rev.* **143**, 365 (1966).
  - <sup>26</sup> E.T. Kulatov, Y.A. Uspenskii, and S.V. Halilov,

- J.Magn.Magn.Mat. **163**, 331 (1996).
- <sup>27</sup> J.L. Dormann, F.D. D'Orazio, F. Lucari, E. Tronc, P. Prene, J.P. Jolivet, D. Fiorani, R. Cherkaoui, and M. Nogues, Phys.Rev.B **53**, 14291 (1996).
- <sup>28</sup> F. Wiekhorst, J. Kötzer, unpublished.